



Optical Stimulation Luminescence Dating of Deltas Revealed the Early to Mid-Holocene Lake-level Fluctuations of Daihai, Inner Mongolia, Northern China

Shixin Huang^{1,2,3} and Xi Chun^{1,4*}

¹Inner Mongolia Restoration Engineering Laboratory of Wetland Eco-Environment System, Inner Mongolia Normal University, Hohhot, China, ²State Key Laboratory of Lake Science and Environment, Nanjing Institute of Geography and Limnology, Chinese Academy of Sciences, Nanjing, China, ³University of Chinese Academy of Sciences, Beijing, China, ⁴Laboratory of Mongolian Plateau Environment and Global Change, Inner Mongolia Normal University, Hohhot, China

OPEN ACCESS

Edited by:

Xiangjun Liu,
Northwest Normal University, China

Reviewed by:

Yiwei Chen,
Chinese Academy of Sciences (CAS),
China
Fuyuan An,
Qinghai Normal University, China

*Correspondence:

Xi Chun
chunxi@imnu.edu.cn

Specialty section:

This article was submitted to
Quaternary Science, Geomorphology
and Paleoenvironment,
a section of the journal
Frontiers in Earth Science

Received: 30 April 2021

Accepted: 21 June 2021

Published: 27 July 2021

Citation:

Huang S and Chun X (2021) Optical
Stimulation Luminescence Dating of
Deltas Revealed the Early to Mid-
Holocene Lake-level Fluctuations of
Daihai, Inner Mongolia,
Northern China.
Front. Earth Sci. 9:702843.
doi: 10.3389/feart.2021.702843

Lake-level reconstruction of inland enclosed lakes especially for monsoon-sensitive areas is of great significance to reveal regional climate changes. Daihai, a typical enclosed lake at the marginal of the East Asian summer monsoon (EASM) area in north China, is sensitive to climate changes due to its unique regional characteristics. There were a series of lakeshore terraces, highstand lacustrine sediments, and braided river deltas, providing sufficient geomorphologic and stratigraphic evidence for the reconstruction of lake-level fluctuations of Daihai. Reconstructed lake-level variations during the early and mid-Holocene were constructed based on 22 quartz optical stimulated luminescence (OSL) ages from six well-preserved profiles around Daihai Basin. Our results indicated Daihai showed a relatively low level at 10.2 ka, and a gradually increasing lake level following the enhanced monsoon precipitation during the mid-Holocene. Specifically, the high lake level began to develop at 8.1 ka and reached the maximum at 5.2 ka, with ~40 m higher than present. At this time, the lake area expanded to ~400 km², approximately six times as large as that of present, corresponding to the maximum monsoon precipitation and intensity of EASM during the mid-Holocene. However, our stratigraphic records showed a part of the depositional records in the north and east of the Daihai was missed after 5.2 ka, probably indicating a sudden drop of the Daihai lake level. These rapid level fluctuations were likely to be interpreted by some local scenarios and need to be further investigated in the future. Overall, the lake-level fluctuation of Daihai during the early and mid-Holocene was slightly different from that observed in the previously published regional records. Possibly, the interaction of the EASM and regional feedback from topography, and hydrology factors might have contributed to the spatial complexity and distinction.

Keywords: lake-level fluctuation, high lake level, early to mid-Holocene, fluvial delta, optical stimulation luminescence, East Asian summer monsoon, monsoon precipitation

INTRODUCTION

Exploring the evidence of the past global climate change in environment-sensitive regions and obtaining its underlying mechanisms are of great significance for the scientific prediction of future climate change (International Geosphere-Biosphere Programme, IGBP). There are large numbers of inland enclosed lakes near the East Asian monsoon margin of China which are highly sensitive to climate change due to its unique regional characteristics. Thus, their lake-level fluctuations are the most direct indicators of regional precipitation and moisture variability related to the intensity of monsoon activities and climate change (Liu et al., 2015; Li et al., 2020a). However, increasing high-resolution lacustrine deposit records have revealed that the lake-level fluctuations during the early and mid-Holocene in East Asian monsoon marginal regions were quite different; especially, the timing of the high lake level in different lakes was asynchronous, and even the same lake might be distinct based on the different dating methods or different materials and proxies.

Inner Mongolia is at the East Asian summer monsoon (EASM) fringe region, the arid/semiarid climate transition zone, and the ecosystem fragile zone in north China. The unique characteristics of the interlaced nomadic with agricultural civilization make it the most sensitive and typical region responding to global climate change. Daihai is a typical inland enclosed lake in Inner Mongolia, whose lake-level fluctuations are of great significance to indicate the regional climate change. A series of research works have focused on the lake-level fluctuations and climate change based on the deposit of lakeshores and drilling cores in Daihai, presenting many valuable literatures and some representative opinions (Wang et al., 1990; Xiao et al., 2004; Peng et al., 2005; Sun et al., 2006). However, there are still many discrepancies and arguments, even conflicts with regard to climate change patterns among them, especially on the timing of highstand records.

Sedimentary records based on the radiocarbon dating in Daihai revealed the high lake level during the early and mid-Holocene. For instance, core sediments and lacustrine sediments from the surrounding terraces revealed that the Holocene climate optimum in Daihai has already begun at 11.5 Cal ka B.P. (10 ka B.P.) and ended at ca. 5.2 Cal ka B.P. (4.5 ka B.P.), corresponding to the termination of the last high lake level (Wang et al., 1990). Lake terrace records indicated that the lake level has increased since 8.8 Cal ka B.P., followed by the highstands at 8.3–7.8 ka B.P. (Li et al., 1992). Meanwhile, monsoon precipitation in Daihai reached its maximum during the mid-Holocene, with an annual precipitation greater than 550 mm (Peng et al., 2005; Xu et al., 2010; Wang et al., 2013), and the warm and humid climate promoted the development of vegetation in Daihai Basin during the mid-Holocene (Jin et al., 2004; Sun and Xiao, 2006; Du et al., 2013). Whereas there was a cold and wet episode at 7.9–7.2 Cal ka B.P. (Xiao et al., 2004; Xu et al., 2004), the lake level frequently fluctuated with a decreasing trend during 10.6–10.0, 9.6–9.0, 7.0–6.3, 5.8–5.2, and 4.5–3.7 Cal ka B.P. inferred from nearshore grain size compositions (Xiao et al., 2013). Moreover, reconstructed lake-level fluctuations based on the

^{14}C dating of lake terraces and sediment cores demonstrated a similar trend that the Daihai lake level expanded temporarily at 10–9 Cal ka B.P. followed by a decreased lake level; thereafter, the lake expanded again during 7.3–3.2 Cal ka B.P. with abundant effective precipitation and superior hydrothermal condition (Sun et al., 2009; Sun et al., 2010). The conclusions above based on the different research carriers are slightly distinct, but all of them presented the increased lake level of Daihai during the early Holocene, and then the development of the high lake level during the mid-Holocene or late mid-Holocene, indicating climate optimum. However, Jin et al. (2013) proposed a temporary expansion of Daihai at 7.5–7.0 Cal ka B.P. and then reached a high lake level at 6.1–2.5 Cal ka B.P. due to the increasing intensity of the monsoon, with a water depth of ~65 m, 35–40 m higher than the present, revealing the development of highstands in Daihai during the late Holocene.

Similarly, the arguments and discrepancies on the occurrence of the high lake level also exist in other lakes in Inner Mongolia. Huangqihai Lake is also located in the middle-east of Inner Mongolia and only 50 km away from Daihai. Sedimentary records based on the ^{14}C dating revealed the Huangqihai Lake developed the high lake level with >70 m higher than modern lake surface during the mid-Holocene (Li et al., 1992; Shen et al., 2006). However, the geological evidence combined with the high-resolution OSL geochronology indicated that warm and wet climate were prevalent during the early Holocene with a stable high lake level, reaching a peak elevation of ~1,340 m, >77 m higher than that present (Zhang et al., 2011; Zhang et al., 2012; Zhang et al., 2016). Subsequently, the lake surface shrank sharply, and the Great Lakes period ended (Xu et al., 2012). Sedimentary records of Dali Lake in eastern Inner Mongolia showed that the high lake level developed in the early and mid-Holocene, with ~60 m, increased of the lake level in 400 years and the triple annual precipitation, followed by the abrupt termination of Holocene humid conditions at 6.3 Cal ka B.P. (5.5 ka B.P.) with a declined lake level of approximately 35 m (Goldsmith et al., 2017). Another sediment core record also demonstrated Dali Lake developed a high lake level due to temperature rise, and glaciers melt during the early and mid-Holocene (11.5–7.6 Cal ka B.P.) (Xiao et al., 2008; Xiao et al., 2009). However, reconstructed lake-level fluctuations based on the OSL dating of beach ridges of Dali Lake reflected the lower lake level related to the reduced monsoon precipitation from 12 to 7 ka and the high lake level with a maximum monsoon precipitation during 7–5 ka (Jiang et al., 2020). In addition, lakes in eastern Inner Mongolia also revealed the distinct timing of highstands. Depositional records of Hulun Lake located in northeastern Inner Mongolia demonstrated that Hulun Lake developed a high lake level during the deglacial and early Holocene (Zhang and Wang, 2000), and thereafter, the secondary high lake level developed again during the mid-Holocene (Liu et al., 2016). Reconstructed lake-level fluctuations in Chagan Nur, an enclosed lake located in eastern Inner Mongolia at the fringe of the modern EASM region, showed a lake highstand of 15–12 m higher than that present at 11–5 ka, with a maximum precipitation of 30–50% higher than that present at 8–6 ka (Li et al., 2020a). Similarly, the depositional records of Juyanze and Zhuyeye terminal lakes on the Alashan

Plateau in western Mongolian plateau indicated that the high lake level developed in the early Holocene and gradually disintegrated at 7–5 Cal. ka B.P. (Chen et al., 2003), but on the contrary, based on topographic and geomorphological analyses, combined with OSL dating results, the high lake level of Zhuyeze Lake appeared in the 8–5 ka with 20 m higher than the modern lake level (Long et al., 2012).

Previous studies on lake-level reconstruction and the timing of the high lake level during the Holocene were distinct even with conflict based on the different research materials and carriers, combined with the different dating methods. They mostly emphasized the analysis of lake cores' sediments to reconstruct the lake-level fluctuation, but there was a lack of the most direct geological and geomorphological evidence. Generally, the research of lake-level fluctuations mainly based on the lake drilling cores and the lakeshore deposition records. Core records can provide relatively continuous high-resolution sedimentary records and the details of lake surface fluctuations to a certain extent, but in terms of the high lake level, the lakeshores, spits, river deltas, and highstand lacustrine sediments retained around the lake are usually used as the good geomorphological evidence to directly indicate high lake-level variations (Wang et al., 1990; Yu et al., 2013). High lake level as a symbol of the peak period of lake evolution indicates the regional warm and humid climate environment, which can provide the basic chronological framework and information for climate change. Furthermore, most of the studies of water lake-level fluctuations were based on the limited dating techniques. Recently, optical stimulated luminescence (OSL) dating technology has been widely used in quaternary studies of dating lacustrine sediments (Long et al., 2011; Fan et al., 2012; Fu et al., 2017; Li et al., 2018b), fluvial/alluvial/delta deposits (Zhao et al., 2016; Guo et al., 2017; He et al., 2019; Nian et al., 2019), aeolian dunes (Cao et al., 2012; Costas et al., 2012; Yu and Lai, 2017), loess/paleosol (Roberts, 2008; Stevens et al., 2018; Li et al., 2018a; Wu et al., 2019; Li et al., 2020b), and so on. This technique was extensively used in the dating of lacustrine deposits in arid and semiarid China because of its advantages over radiocarbon dating, which is limited by the so-called reservoir effects. And among those areas with significant reservoir effects, the application of OSL dating also can be used to assess the reservoir effects and calibrate the radiocarbon dating results (Liu and Lai, 2012; Lai et al., 2014).

Consequently, here we investigated the timing of the high lake level during the early-to-mid Holocene based on the OSL dating from Daihai Lake in the margin of EASM in north China. Series of lakeshore terraces, highstand lacustrine deposits, and well-preserved river deltas around the Daihai Basin could provide sufficient sedimentary and geomorphological evidence for the reconstruction of lake-level fluctuations, which is of great significance to reveal the regional climate change. Based on 22 quartz OSL ages, we attempted to reconstruct lake-level fluctuations and figure out the timing of highstands during the early and mid-Holocene, and further discuss the underlying mechanisms of the lake-level fluctuation in Daihai and its response to the variability of EASM intensity during the early and mid-Holocene.

MATERIALS AND METHODS

Study Area

Daihai Basin is located in Liangcheng County of the southeastern Inner Mongolia Plateau, northern China, with complex landforms which are mainly composed of mountains and hilly areas (Figure 1A). Daihai Lake (40°29'27" N–40°37'06" N, 112°33'31" E–112°46'40" E, 1,220 m a.s.l.) is an ellipse-shaped enclosed lake at the lowest point of the basin. The water supply of Daihai mainly depends on atmospheric precipitation, rivers, and surface runoff. Daihai is fed by 22 rivers, most seasonal braided rivers developed on the northern shore, and only those in the western are meandering rivers; among them, five main rivers, Gongba River, Wuhao River, Tiancheng River, Buliang River, and Muhua River, flow into the lake (Shi et al., 2014) (Figure 1B). The lake area is 61.5 km², with a drainage area of 2364.2 km², a maximum depth of 11.5 m, and a mean depth of 6.67 m.

Daihai located in the margin of EASM-influenced regions is mainly dominated by a semiarid moderate temperate continental monsoon climate (Figure 1A). Regional precipitation was mainly delivered *via* EASM transportation (Wang et al., 1990). The meteorological data analysis results of Liangcheng Station in Inner Mongolia from 1960 to 2017 AD demonstrate that the annual average temperature in Daihai Basin was approximately 5.6°C; the annual average precipitation was ~410 mm and ca. 70%; annual precipitation decreased in July–September; the mean annual evaporation reached 1860 mm, four times higher than the annual precipitation; the average of the frost-free period was generally 120 days; Daihai Basin in winter is often affected by Mongolian–Siberian cold air and northwest wind with wind scale ranging from 5 to 8. The annual average wind speed was 2.6 m/s, and the maximum wind speed was up to 15 m/s. In recent decades, the semiarid climatic condition makes the precipitation of Daihai Basin a natural shortage, and then the anthropogenic-induced climate warming and agricultural activities make Daihai rapidly shrink (Liu et al., 2019; Chun et al., 2020).

Daihai Basin is an asymmetric closed rift basin. Because of the fault activities, the slope of the lake basin is different from that of the north and the south, which shows the characteristics of steepness in the north and gentle in the south. Since the formation, Daihai has experienced frequent lake-level fluctuations, and thus, there were many ancient relics left behind and well-preserved lake sedimentary profiles due to its long-term hydrologic closure state.

Sample Collection

Lakeshore terraces at different heights, highstand lacustrine deposits, fluvial terraces, and river deltas are widely distributed around the Daihai Basin (Wang et al., 1990; Sun et al., 2009; Yu et al., 2013). There are nine small deltas in the northern steep slope of Daihai Basin due to topographic characteristics, and fluvial and seasonal floods, such as Yuanzigou Delta; only two but big deltas were distributed in the southern gentle slope (Buliang River Delta and Tiancheng River Delta); the largest Muhua River

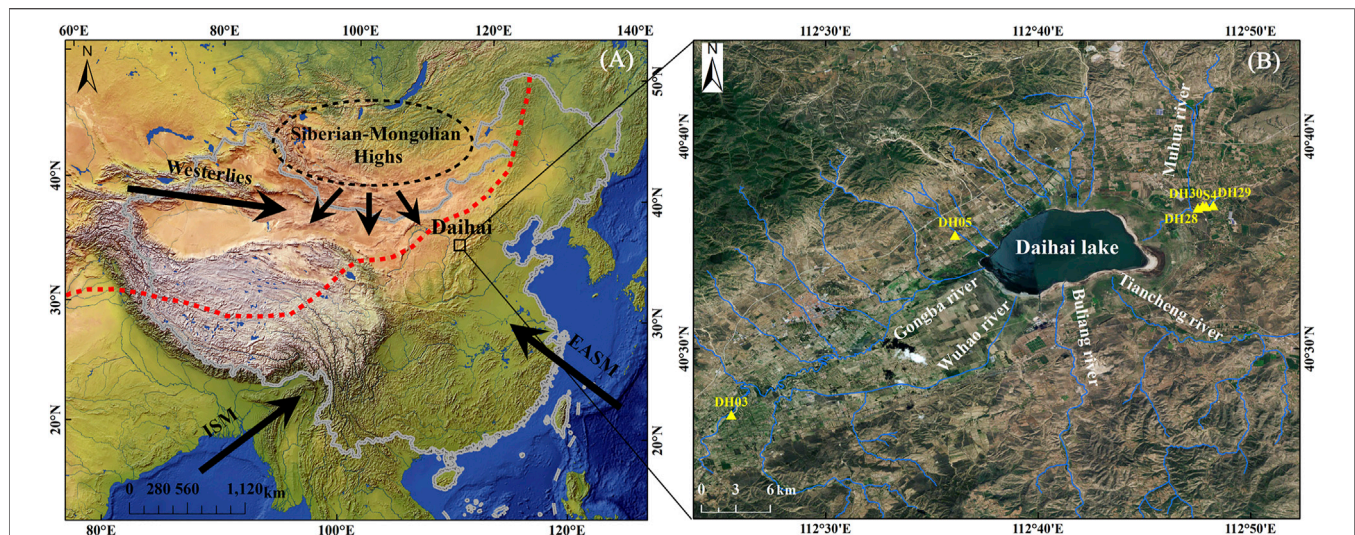


FIGURE 1 | Geographical map of the study area showing (A) the location of the Daihai Lake Basin and atmospheric circulation systems of China [i.e., Indian summer monsoon (ISM), East Asian summer monsoon (EASM), Westerlies, and Siberian–Mongolian High winter monsoon], the red dash line represents the modern northern boundary of the EASM according to Chen et al. (2008), and (B) sampling sites around the Daihai lake basin based on the Map World (<https://www.tianditu.gov.cn/>).

(braided river) delta in the eastern Daihai and Gongba River (meandering river) delta in the western area (Yu et al., 2013). Thus, the braided river delta plains were formed on the north, south, and east coast of Daihai, while the meandering river delta plain only developed in the west. The formation of the braided river deltas was determined by the construction of the braided river plain entering the lake and the wave action of the lake. The basin tectonic activity, seasonal flood intensity, and lake-level fluctuations are the main factors to control its development, so braided river deltas can be used as the most intuitive indicator of lake-level fluctuations in Daihai (more details in Supplementary Material and Supplementary Figure S1).

By conducting field geomorphic investigations around the Daihai Basin, we collected OSL age samples at six sites from the west to east of Daihai Basin (Figure 1B). DH03 section is a fluvial terrace in Gongba River catchment, western Daihai. DH05 section is located in Yuanzigou Delta, northern Daihai. DH28, DH29, and DH30 sections are located in Muhua River Delta, eastern Daihai. The Yuanzigou delta is a braided river delta with the steep slope in a near-source transportation way, while the Muhua River Delta is far away from the source with fine grains of good abrasion. The way they entered the lake mainly depended on the seasonal floods and rainfalls. Differential global positioning system (DGPS) was used to measure elevations during field investigation, and the elevation of each section was further determined by a 1:50,000 topographic map of Liangcheng County combined with Google Earth.

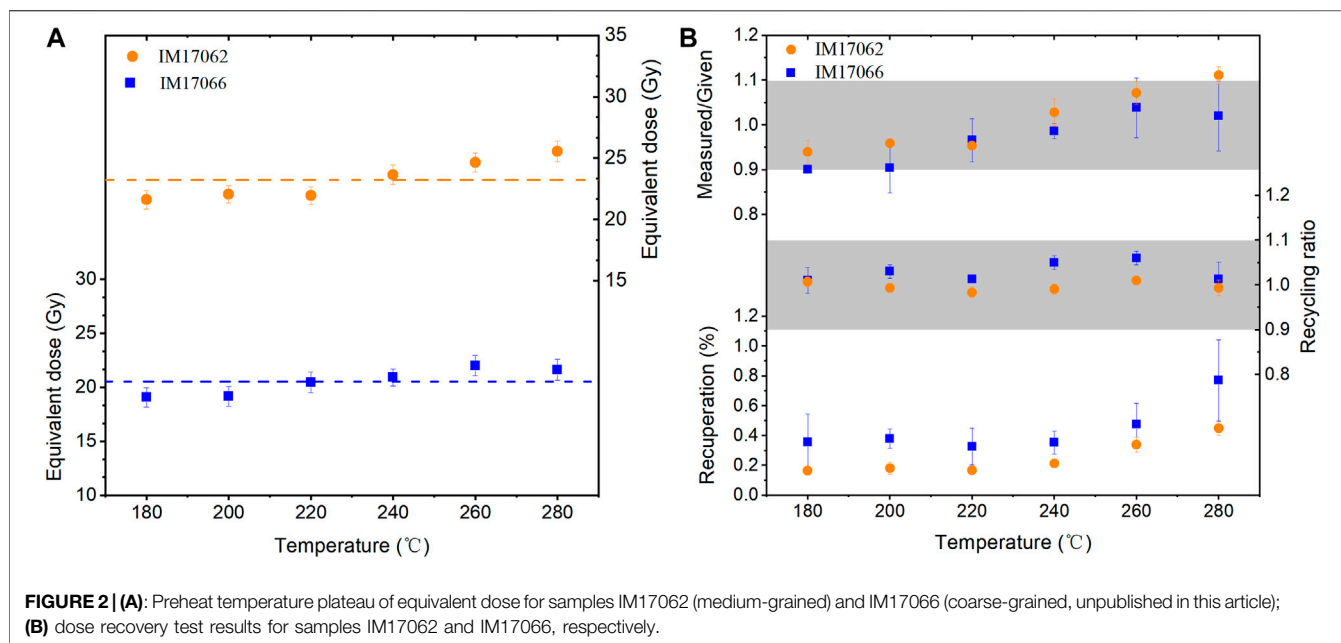
Grain Size Pretreatment

Pretreatment of grain size was performed according to the method proposed in the study by Peng et al. (2005). Samples in beakers were treated with 10 ml of 30% H₂O₂ and 10 ml of 10% HCl to remove the organic matter and carbonate, respectively; the

beakers were filled with deionized water, maintained for 24 h, and acidic ions were removed until the solution was nearly neutral (PH = 7); sample residues were deflocculated with 10 ml of 0.05 mol/L (NaPO₃)₆ with an ultrasonicator for 15 min to facilitate dispersion and eliminate the sample cementation. The grain size of prepared samples was measured and analyzed by Malvern Mastersizer 3000 analyzer with a measurement range of 0.01–3,500 μm. The repeated measurement error was less than 2%.

Optical Stimulated Luminescence Dating

A total of 22 OSL samples from six sections around Daihai Basin were taken from the freshly prepared vertical profiles by using light-tight steel tubes and were sealed on sites to prevent light exposure and moisture loss for luminescence dating. Sample preparations and measurements were performed in the Laboratory of Mongolian Plateau Environment and Global Change, Inner Mongolia Normal University. Under the subdued red light conditions, the outer materials at the ends of each tube were reserved for the measurement of water content and the environmental dose rate, and the unexposed materials at the middle part of the tubes were treated with 10% HCl and 30% H₂O₂ to remove carbonates and organic material, respectively. Samples were wet-sieved to select medium-grained (MG, 38–63 μm) or coarse-grained (CG, 63–90 μm or 90–125 μm) fractions and then separated using heavy liquids calibrated to the density of 2.72 and 2.62 g cm⁻³ to remove heavy minerals and extract quartz grains, respectively. Afterward, the CG quartz fractions were etched with 40% HF for 40 min to dissolve feldspars and the outer alpha-irradiated surface. The MG quartz fractions were etched with H₂SiF₆ for 1–2 weeks. The etched samples were rinsed with 1 mol/L HCl to remove fluoride precipitates, and then washed with distilled water. The purity of the isolated quartz was checked using the infrared light



stimulation (IR checking), and samples with the OSL-IR depletion ratio deviated from 10% of unity were retreated again (Duller, 2003).

OSL measurements were performed using an automated Risø TL/OSL DA-20 reader, equipped with a calibrated $^{90}\text{Sr}/^{90}\text{Y}$ beta source (Botter-Jensen et al., 2010) with a dose rate of ~ 0.115 Gy/s. We used blue light LED ($\lambda = 470 \pm 30$ nm) stimulation for quartz and infrared LED ($\lambda = 830$ nm) stimulation for IR depletion ratio check. Quartz OSL signal was detected through a 7.5-mm Hoya U-340 filter. A standard single aliquot regenerative-dose (SAR) protocol was applied for pretests and equivalent dose (D_e) measurements (Supplementary Table S1) (Murray and Wintle, 2000; Wintle and Murray, 2006).

The concentration of radioactive nuclides (U, Th, and Rb) was measured by inductively coupled plasma mass spectrometry (ICP-MS; Thermo iCAP RQ), while the content of K (%) was determined by inductively coupled plasma optical emission spectrometry (ICP-OES; Thermo iCAP 7400). The environment external dose rate determination was based on the U, Th, K, and Rb concentrations from bulk samples. An alpha efficiency factor (α -value) of 0.035 ± 0.003 was used for the aging calculation of 38–63 μm quartz grains (Lai and Brueckner, 2008). The CG quartz fractions were etched to remove the outer alpha-irradiated layer, and thus circumvent the necessity to determine the alpha dose and alpha dose effectiveness. The attenuation factors of Brennan et al. (1991) and Guerin et al. (2012) were used to calculate the alpha and beta dose rates, respectively. The contribution of cosmic ray was calculated using the buried depth of the samples, altitude, and geomagnetic latitude following the reference (Prescott and Hutton, 1994). Based on the local deposited environment, previous research (Li et al., 2020a), and measured and saturated water content of these samples, the water content of $10 \pm 5\%$ was assumed in the aging calculation. The total dose

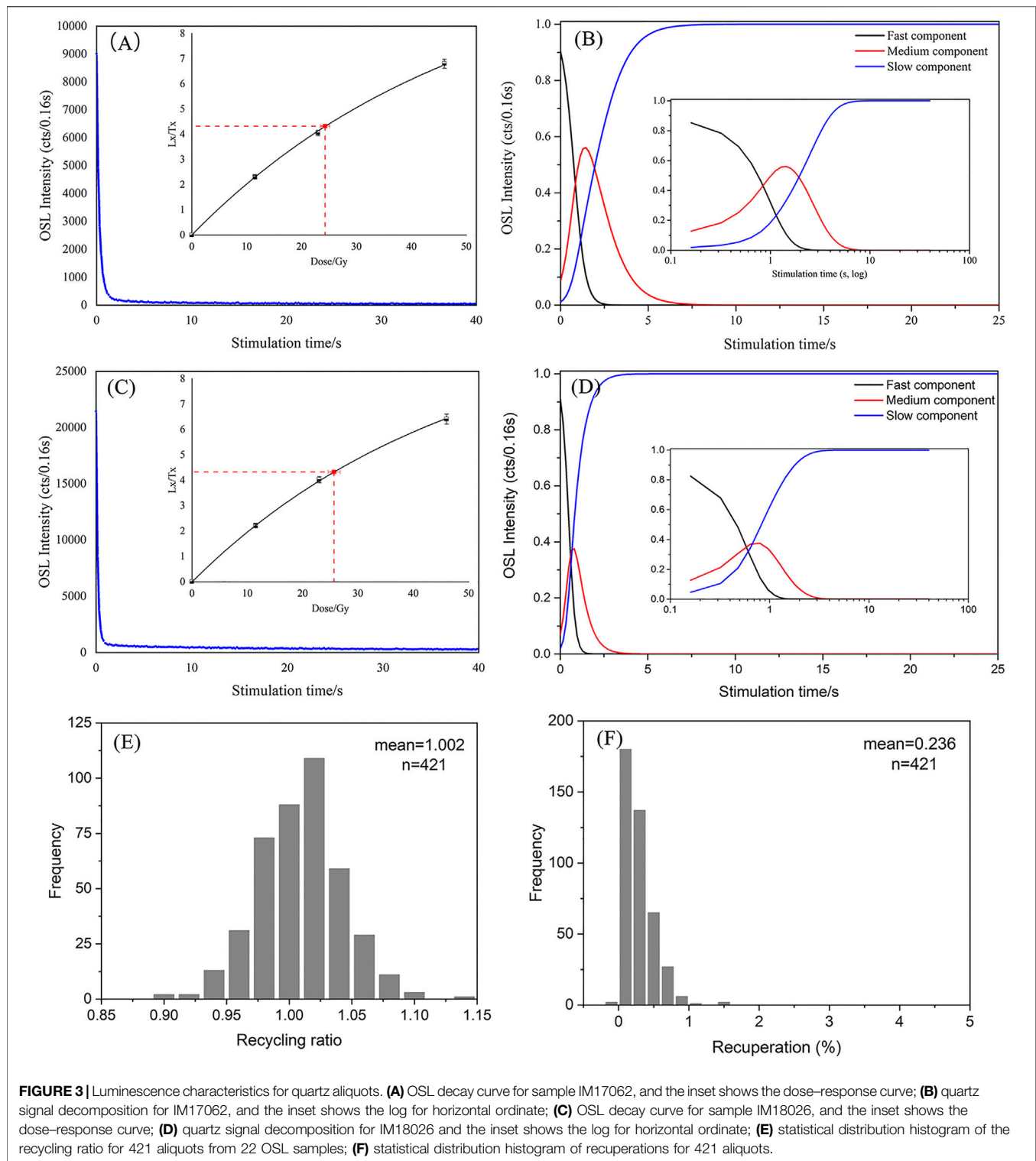
rates were finally calculated using the functions defined by Aitken (1985); Aitken (1998).

RESULTS

D_e Determination, Luminescence Characteristics, and Geochronology

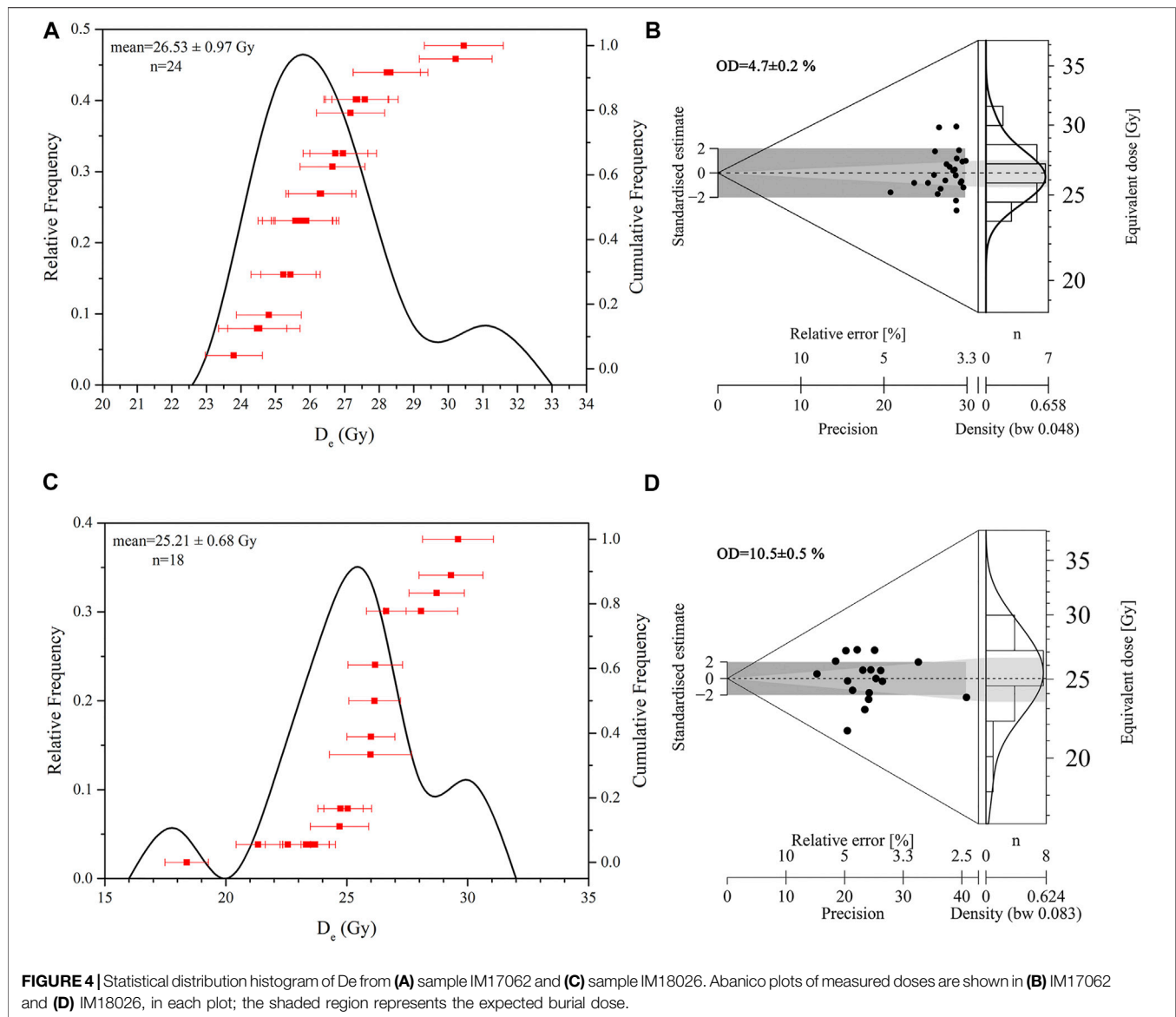
All the samples have a thermal luminescence (TL) peak at 110°C , and the IR-depletion ratio ranges between 0.9 and 1.1 (Supplementary Figures S2, S3), indicating the prevention of the measured signals of quartz grains from feldspar contamination, which meets test requirements (Thomsen et al., 2008). To select an appropriate thermal treatment, preheat plateau tests were carried out on both MG quartz (IM17062) and CG quartz (IM17066; unpublished in this article, but this sample was taken from the sampling site near the DH05) before the D_e measurement. The preheat plateau test was carried out by dividing the aliquots into six groups, with preheat temperatures ranging from 180 to 280°C with a 20°C increment. The observed D_e plateau from 180 to 280°C indicated that D_e values are rather insensitive to the preheat temperature; both samples present a good D_e plateau (Figure 2A). As shown in Figure 2B, constrained by acceptable range (0.9–1.1) of the recycling ratio and negligible recuperations (lower than 5%), the dose recovery ratio is consistent with unity within the 1σ error for all the preheat temperatures (Murray and Olley, 2002). Finally, a preheat temperature of 240°C with a cut-heat of 200°C was chosen for the D_e measurements of all the samples of Daihai.

The decay curves obtained from sample MG quartz (IM17062) and CG quartz (IM18026) are shown in Figures 3A,C, with typical dose–response curves inset. The decay curves were



decomposed into three components: fast component, medium component, and slow component by curve fitting (**Figures 3B,D**) (Bailey et al., 1997). As shown in **Figure 3**, the OSL signals rapidly decay to the background, indicating the domination of the fast component in the quartz signal, and the signal can be sufficiently

bleached in a very short time, which can be seen in the same characteristics in all samples in this study. The average recycling ratio of 421 aliquots from 22 samples is 1.002 (**Figure 3E**), confirming that the sensitivity corrections work well, and the measurements following the laboratory irradiations are



reproducible. The recuperations from 421 aliquots are all less than 2% (Figure 3F), showing the negligible thermal transfer effects (Wintle and Murray, 2006). The D_e distributions of both MG (IM17062) and CG (IM18026) quartz are quite narrow, with small over-dispersion (OD) values (4.7 ± 0.2 and $10.5 \pm 0.5\%$, respectively) (Figure 4), indicating the samples were well bleached before burial (Arnold and Roberts, 2009). Almost all samples showed similar luminescence characteristics and the normal distributions for the D_e values. All above suggest the suitability of the SAR protocol in D_e determination of quartz OSL sedimentary samples in Daihai and the reliability of dating results.

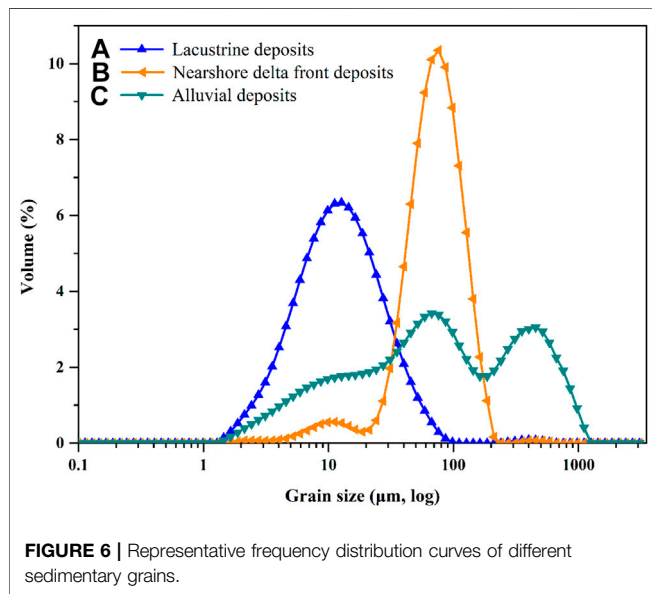
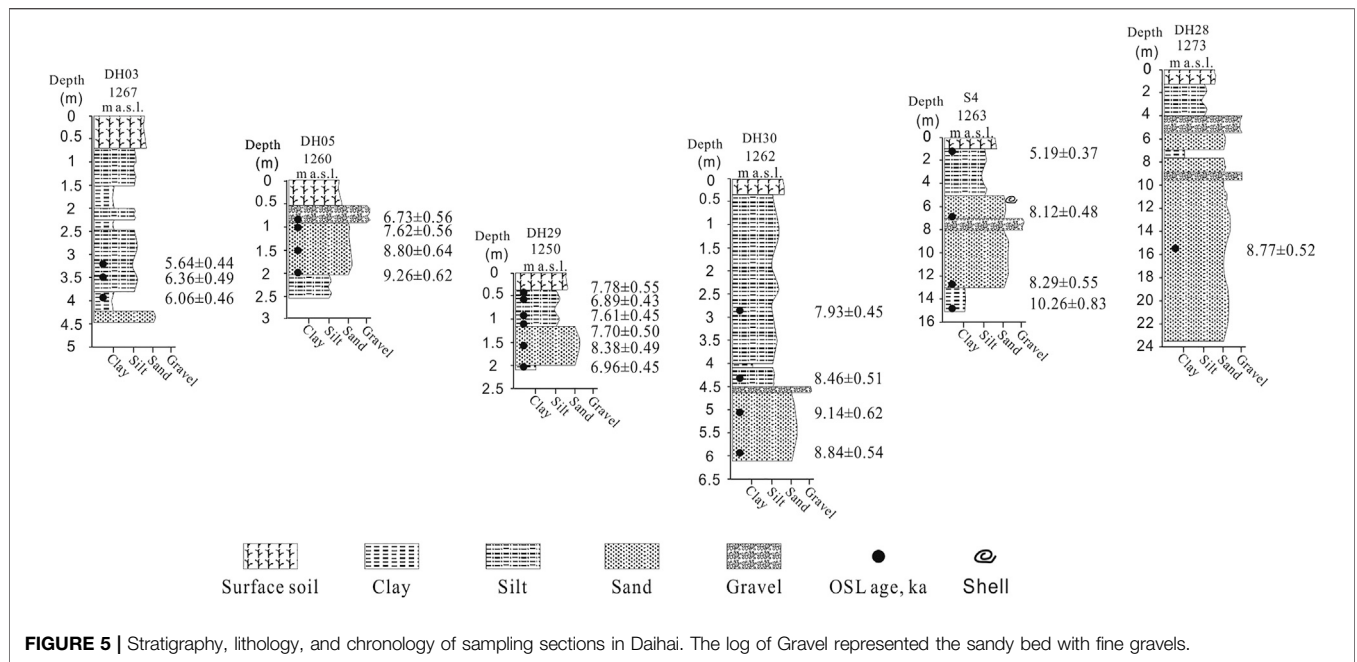
The dating results of 22 OSL samples collected from six sections in this article are listed in Table 1. The stratigraphy and OSL sampling sites are illustrated in Figure 5. The dating ages are almost consistent with the deposition depth within the error range.

Grain Size Characteristics and Sedimentary Environments of the Sedimentary Sections

Sediment grain size composition and distribution patterns can reflect the hydrodynamic conditions, the sedimentary environment, and depositional processes to some extent (Ding et al., 2001). The ternary diagram of grain size shows (Supplementary Figure S4) that sediments were mainly composed of silt (4–63 μm), whereas sand (>63 μm) accounted for a large proportion in some samples of the DH29 and DH30 sections, whose geochronology mainly ranges from 9 to 7 ka. The median size of sediments varied obviously in different deposition periods. At 6.5–5.2 ka, sediment compositions were dominated by fine silt (7.8–15.6 μm). The frequency distribution curves can provide more detailed information on the sedimentary environment. Consequently, combined with the stratigraphic field investigation and the previous research works (Xiao et al.,

TABLE 1 | Summary of quartz OSL dating results from Daihai Basin.

Sample ID	Depth (cm)	Aliquots	Grain size (μm)	De (Gy)	OD (%)	U (ppm)	Th (ppm)	K (%)	Cosmic rate	Dose rate (Gy/ka)	W.C. (%)	Age (ka)
IM17001	1,500	24	63–90	26.51 \pm 1.55	19.8 \pm 0.6	1.72 \pm 0.08	7.56 \pm 0.24	1.79 \pm 0.06	0.06	2.58 \pm 0.14	10 \pm 5	10.26 \pm 0.83
IM17002	1,300	19	63–90	28.37 \pm 0.97	12.9 \pm 0.6	0.68 \pm 0.04	2.29 \pm 0.11	3.26 \pm 0.09	0.07	3.42 \pm 0.19	10 \pm 5	8.29 \pm 0.55
IM17003	700	22	63–90	20.58 \pm 0.46	8.7 \pm 0.4	1.7 \pm 0.08	7.44 \pm 0.24	1.69 \pm 0.06	0.11	2.53 \pm 0.14	10 \pm 5	8.12 \pm 0.48
IM17004	100	22	63–90	15.17 \pm 0.76	22.0 \pm 0.7	1.18 \pm 0.06	8.29 \pm 0.26	2.03 \pm 0.06	0.22	2.93 \pm 0.15	10 \pm 5	5.19 \pm 0.37
IM17062	395	24	38–63	26.53 \pm 0.34	4.7 \pm 0.2	4.60 \pm 0.50	16.29 \pm 0.70	2.06 \pm 0.04	0.13	4.37 \pm 0.33	10 \pm 5	6.06 \pm 0.46
IM17063	350	23	38–63	23.55 \pm 0.39	6.5 \pm 0.3	2.84 \pm 0.40	14.00 \pm 0.70	2.00 \pm 0.04	0.14	3.70 \pm 0.28	10 \pm 5	6.36 \pm 0.49
IM17064	320	24	38–63	15.23 \pm 0.20	5.4 \pm 0.2	1.82 \pm 0.30	8.20 \pm 0.60	1.65 \pm 0.04	0.15	2.70 \pm 0.21	10 \pm 5	5.64 \pm 0.44
IM17074	200	22	90–125	31.78 \pm 1.30	16.1 \pm 0.6	1.52 \pm 0.30	13.18 \pm 0.7	2.21 \pm 0.04	0.20	3.43 \pm 0.18	10 \pm 5	9.26 \pm 0.62
IM17075	150	18	63–90	30.10 \pm 1.52	19.8 \pm 0.8	1.39 \pm 0.3	12.94 \pm 0.7	2.20 \pm 0.04	0.21	3.42 \pm 0.18	10 \pm 5	8.80 \pm 0.64
IM17076	100	18	90–125	26.34 \pm 1.38	21.0 \pm 0.9	1.36 \pm 0.30	12.50 \pm 0.70	2.28 \pm 0.04	0.22	3.45 \pm 0.18	10 \pm 5	7.62 \pm 0.56
IM18001	90	18	90–125	25.12 \pm 1.61	24.2 \pm 1.0	1.44 \pm 0.30	15.35 \pm 0.70	2.35 \pm 0.04	0.23	3.73 \pm 0.2	10 \pm 5	6.73 \pm 0.56
IM18017	40	16	90–125	23.20 \pm 1.12	17.4 \pm 0.8	1.16 \pm 0.30	6.87 \pm 0.60	2.18 \pm 0.04	0.26	2.98 \pm 0.15	10 \pm 5	7.78 \pm 0.55
IM18018	60	18	90–125	25.47 \pm 0.84	14.8 \pm 0.6	1.11 \pm 0.30	12.37 \pm 0.70	2.58 \pm 0.04	0.24	3.70 \pm 0.19	10 \pm 5	6.89 \pm 0.43
IM18019	90	18	90–125	27.52 \pm 0.70	9.2 \pm 0.4	0.75 \pm 0.30	5.61 \pm 0.60	3.07 \pm 0.05	0.23	3.62 \pm 0.19	10 \pm 5	7.61 \pm 0.45
IM18020	120	17	90–125	27.07 \pm 1.04	14.2 \pm 0.6	1.18 \pm 0.30	6.89 \pm 0.60	2.79 \pm 0.04	0.22	3.51 \pm 0.18	10 \pm 5	7.70 \pm 0.50
IM18021	160	18	90–125	24.57 \pm 0.64	10.1 \pm 0.4	1.91 \pm 0.30	10.09 \pm 0.70	1.80 \pm 0.04	0.21	2.93 \pm 0.15	10 \pm 5	8.38 \pm 0.49
IM18022	210	15	63–90	23.48 \pm 0.89	13.7 \pm 0.7	2.92 \pm 0.40	12.92 \pm 0.70	1.85 \pm 0.04	0.19	3.37 \pm 0.18	10 \pm 5	6.96 \pm 0.45
IM18023	280	18	63–90	22.23 \pm 0.44	7.0 \pm 0.4	1.97 \pm 0.30	9.47 \pm 0.60	1.71 \pm 0.04	0.18	2.81 \pm 0.15	10 \pm 5	7.93 \pm 0.45
IM18024	430	15	90–125	24.35 \pm 0.62	8.2 \pm 0.5	2.60 \pm 0.40	7.86 \pm 0.60	1.83 \pm 0.04	0.15	2.88 \pm 0.16	10 \pm 5	8.46 \pm 0.51
IM18025	510	18	90–125	27.90 \pm 1.15	14.4 \pm 0.6	1.99 \pm 0.30	10.59 \pm 0.70	1.96 \pm 0.04	0.14	3.05 \pm 0.16	10 \pm 5	9.14 \pm 0.62
IM18026	590	18	90–125	25.21 \pm 0.68	10.5 \pm 0.5	2.27 \pm 0.40	7.87 \pm 0.60	1.89 \pm 0.04	0.13	2.85 \pm 0.16	10 \pm 5	8.84 \pm 0.54
IM18031	1,540	16	90–125	32.16 \pm 0.73	8.6 \pm 0.4	1.86 \pm 0.30	11.26 \pm 0.70	2.68 \pm 0.04	0.05	3.67 \pm 0.20	10 \pm 5	8.77 \pm 0.52



2013), we designed frequency distribution curves as three types in this article: (A) lacustrine deposits, (B) nearshore delta deposits, and (C) alluvial/fluviial deposits (Figure 6).

DH03 section is located in the west of Daihai (1,267 m a.s.l.) and was identified as typical fluvial deposition (Supplementary Figure S5A), and it mainly comprised fine silt accounting for 69.8–89.8%, and the frequency distribution curves show a single peak with positive skewness (Supplementary Figure S6A). During 6.4–5.6 ka, the Gongba River with stronger hydrodynamic force carried a large number of loess around and then deposited here with a high sedimentation rate, and with frequent alluvial transformations, which indicates humid

climate and increased precipitation in the Daihai Basin at 6.4–5.6 ka.

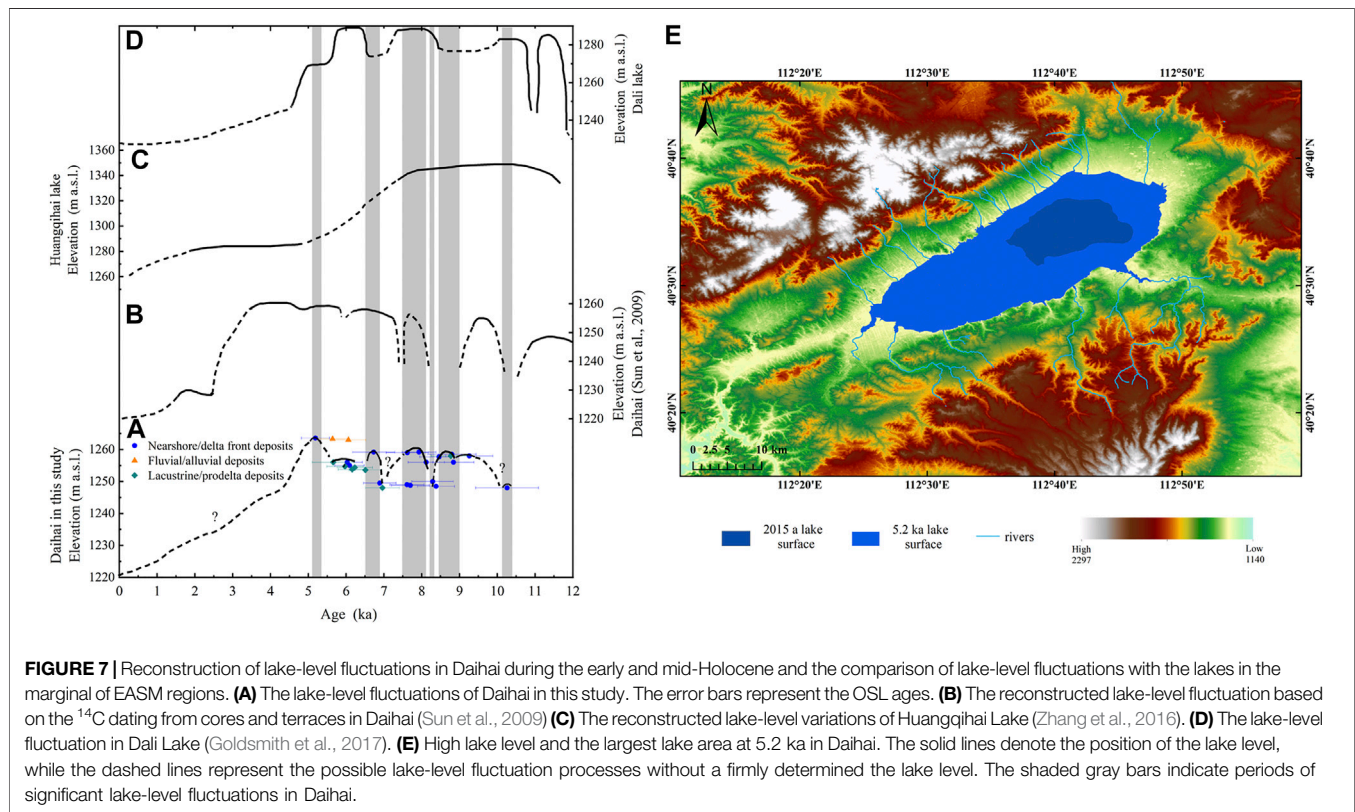
The frequency distribution curves of samples in DH05 section are bimodal distribution with a main peak at the fine sand grains and the secondary peak at 859 μm at 7.62 ± 0.56 ka (Supplementary Figure S6B), which indicated the heavy rainfalls with alluvial deposits [Type (C) in Figure 6], carrying a massive of coarse grains from lakeshores into the lake. At 9.2–6.7 ka, the frequency curves present a single peak with leptokurtosis [Type (B) in Figure 6]. The main components of sediments were silt, and the delta front developed with small sandy mixed bedding (Supplementary Figure S5B).

The frequency distribution curves of samples in DH29 section (Supplementary Figures S5C, S6C) revealed the depositions of the delta front during 8–7 ka. Meanwhile, wave action with wind transported a large number of coarse grains into the lake. Thereafter, the lake began to expand at 6.96 ± 0.45 ka, and pro-delta developed, indicating a transition to the deep lake phase. The frequency distribution curves of samples in DH30 and Supplementary Figure S4 section (Supplementary Figures S6D,E) also indicated the delta front developed during 9–8 ka. Consequently, sections DH05, DH26, DH29, and DH30 were recognized as the braided river delta depositions to indicate the fluctuations of the lake level.

The frequency distribution curves of samples in DH28 section (Supplementary Figure S6F) displayed shallow lacustrine deposits with a secondary peak of coarse grains, which indicated highstand lacustrine deposits here with a relative high lake level at 8.77 ± 0.52 ka.

Lake-Level Reconstruction of Daihai During the Early-to-Mid Holocene

Based on the quartz OSL dating results and elevations of typical lakeshore/fluviial terraces and braided river deltas preserved in the



sections around Daihai, we reconstructed the history of lake-level fluctuations during the early and mid-Holocene (Figure 7A). It is generally considered that the uppermost lacustrine sediments of the terraces were limited to represent the lower water level during that time (Sun et al., 2009). The uppermost delta front depositions could be used to indicate the highest water level once reached. The delta front is affected by the current lake shoreline and is a part of transforming into the delta plain, which can provide a conservative evidence to indicate lake-level fluctuations. Consequently, for the delta front depositions at the same time on different terraces, the highest elevation of the depositions was used to represent the lake level at that time. The pro-delta is regarded as a part of shallow lake, and thus the pro-delta depositions as same as the lacustrine sediments are also used to constrain the lower lake level.

The reconstructed lake-level fluctuation curve showed a relatively low level at 10.2 ka. Thereafter, the lake level may present an upward trend during 10.2–9.2 ka, and then increased to a higher lake level at 9.2–8.8 ka. However, the lake level temporarily rapidly declined at ca. 9.0 ka. Subsequently, the lake level quickly increased to the former water level and remained at a relatively high lake level during 8.8–8.5 ka. While the lake level dropped significantly at 8.5–8.1 ka again, we assumed it was possibly a response to the 8.2 ka cold events (Matero et al., 2017). After the episode, the Daihai lake level gradually increased and remained at a higher lake level at 8.1–5.2 ka, and then reached the optimum at 5.2 ka with the ~40 m higher than the modern lake level, and the lake area expanded to ~400 km², about six times as large as that of present

(Figure 7E). At that time, Daihai Lake extended west to the Sandao Bay and east to the Wayao village, covering a large area of modern cropland. However, the depositional records showed that the lake-level fluctuations between 8.1 and 5 ka were more frequent, and the heavy rainfall events occurred at ca. 6.2 ka and ca. 7.6 ka when surface runoff and rivers carried massive coarse grains and gravel into the lake and then deposited. Our sedimentary records showed that a part of the depositional records in the northern and eastern Daihai (e.g., DH29 and Supplementary Figure S4) was missed after 5.2 ka, and the soil humus layer developed, which may indicate the sudden drop of the Daihai lake level. We inferred that another reason was that the upper lacustrine deposit layer or delta depositions may be eroded after the lake declined, and thus developed into the soil humus layer. Due to the lack of more evidence from the other geomorphic profiles, the specific reasons were largely unknown, but be worthy of further investigation in the future. Thus, here we do not discuss the lake-level fluctuations of Daihai after 5.2 ka.

DISCUSSION

Regional Comparison of Reconstructed Lake-Level Fluctuations at the Fringe of EASM-Influenced Areas

Here, we compared the reconstructed lake-level fluctuations of Daihai in this article with those of Daihai based on the different dating methods and proxies (Sun et al., 2009)

(Figure 7B), and further compared with the reconstructed lake levels of Huangqihai Lake (Zhang et al., 2016) (Figure 7C), and Dali Lake (Goldsmith et al., 2017) (Figure 7D) located in the EASM margin regions during the early-to-mid Holocene. Results demonstrate that Daihai had a relatively lower level at 10.2 ka., which may be a response to Younger Dryas (YD) events. However, it was not recorded in Daihai based on the ^{14}C dating but replaced with an inferred declined lake level. Subsequently, the Daihai lake level was prone to rise at 10.2–9.2 ka, which was also recorded in Figure 7B, and then reached a relatively higher lake level until 9.2–8.5 ka. Thereafter, the lake level underwent a decrease as a response to 8.2 ka cooling event, which crossed large parts of the Northern Hemisphere (Matero et al., 2017). After 8.2 ka cooling event, the Daihai lake level began to increase again and was maintained at a persistent and stable high lake level during 8.1–5.2 ka, except an inferred declined lake level at 7.5 ka. At 5.2 ka, the Daihai lake level reached its maximum, about 40 m higher than the modern lake level. Similar records in Figure 7B also revealed the high lake level during this time. However, our results showed that the high lake level developed at 5.2 ka, and then a sudden declined level occurred after 5.2 ka, while reconstruction results in Figure 7B indicated Daihai expanded on a large scale with the abundant monsoon effective precipitation and humid climate at 8.1 Cal ka B.P. (7.3 ka B.P.), and this persistent and stable high lake-level stage remained until 3.4 Cal ka B.P. (3.2 ka B.P.) (Sun et al., 2009). Overall, our reconstruction results filled the knowledge gap of lake-level variations of Daihai based on the ^{14}C dating of cores and lakeshores.

Lake-level fluctuations displayed in Huangqihai Lake and Dali Lake were slightly distinct with Daihai (Figures 7C,D). Results showed that the Dali lake level was more than 60 m higher than present, with a two-fold increase in annual rainfall during the 8.8–6.3 Cal ka B.P. (8.0–5.5 ka B.P.). At ca. 6.3 Cal ka B.P. (5.5 ka B.P.), the lake level dropped about 35 m, indicating the termination of humid conditions, which triggered a large cultural collapse of Early Neolithic cultures in north China, and possibly promoted the emergence of complex societies of the Late Neolithic (Goldsmith et al., 2017). There were also sub-fluctuations at ca. 10.6–10, 9.6–9, 7–6.3, 5.8–5.2, 4.5–3.7, 3.2–2.7, 2.3–2, 1.7–1.4, and 1.1–0.2 Cal. ka B.P.; the precipitation decreased, and the lake level declined with the decreasing nearshore components of lake sediments (Xiao et al., 2013; Xiao et al., 2015). Lake-level fluctuations of Dali in the Holocene were not only related to the monsoon intensity but also affected by ice and ice melt. Thus, the beginning of the high lake level was slightly earlier than that of Daihai, and the terminal time was also slightly earlier. Lake-level reconstruction of Huangqihai Lake based on OSL dating (Figure 7C) revealed a peak elevation of ~1,340 m (>77 m higher than the present) during the early Holocene, which remained such highstand from ~10 to ~8 ka and retreated toward the middle and late Holocene. The beginning and termination of the high lake level

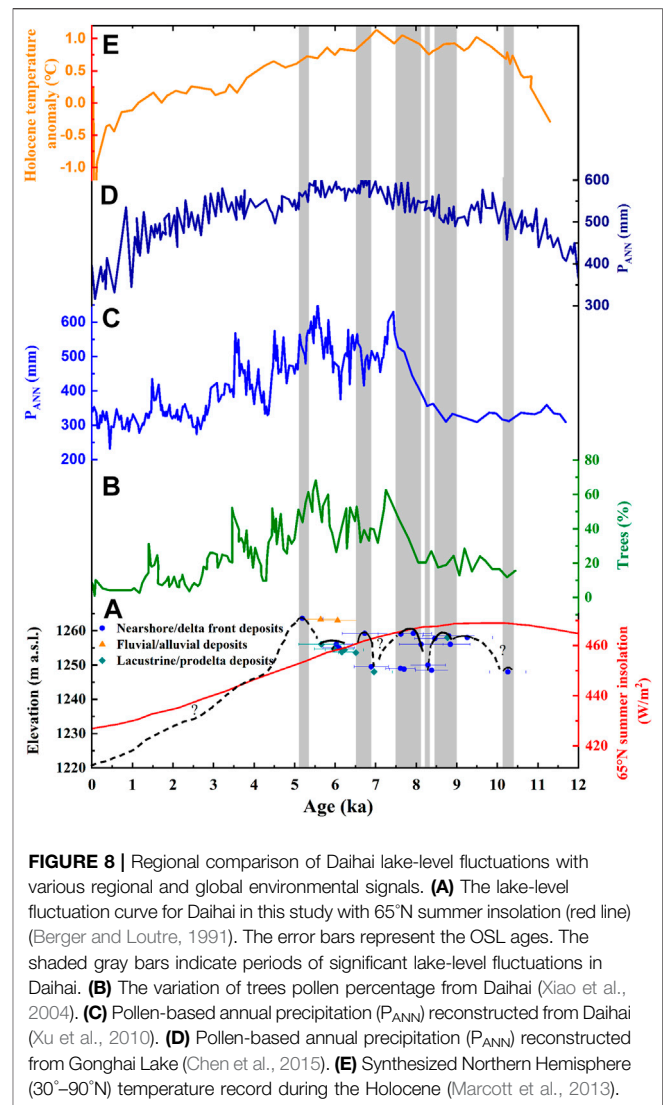


FIGURE 8 | Regional comparison of Daihai lake-level fluctuations with various regional and global environmental signals. **(A)** The lake-level fluctuation curve for Daihai in this study with 65°N summer insolation (red line) (Berger and Loutre, 1991). The error bars represent the OSL ages. The shaded gray bars indicate periods of significant lake-level fluctuations in Daihai. **(B)** The variation of trees pollen percentage from Daihai (Xiao et al., 2004). **(C)** Pollen-based annual precipitation (P_{ANN}) reconstructed from Daihai (Xu et al., 2010). **(D)** Pollen-based annual precipitation (P_{ANN}) reconstructed from Gonghai Lake (Chen et al., 2015). **(E)** Synthesized Northern Hemisphere (30°–90°N) temperature record during the Holocene (Marcott et al., 2013).

from Huangqihai Lake were both much earlier than those of Daihai Lake.

The Underlying Mechanism of lake-level fluctuations of Daihai During the Early and Mid-Holocene

We further compared various regional and global environmental signals to investigate the underlying mechanism of lake-level fluctuations of Daihai Lake or even lakes at the fringe of the EASM regions (Figures 8, 8A). The variation of tree pollen percentage from Daihai (Figure 8B) indicated woody plants showed an increasing trend during the early-to-mid Holocene, which may suggest the humidity gradually increased during 10.2–7.9 Cal. ka B.P., and then there was a large-scale coverage of mixed coniferous and broadleaved forests at 7.9–4.5 Cal. ka B.P., marking the warm and humid climate environment (Xiao et al., 2004). Precipitation variability in Daihai also indicated that the

increasing precipitation at 7.9–3.1 Cal. ka B.P. and reached a higher level at 5.2 ka (Peng et al., 2005). Pollen-based annual precipitation (P_{ANN}) reconstructed from Daihai (Figure 8C) demonstrated that the period of 6.2–5.1 Cal ka B.P. was the wettest and warmest interval, with annual precipitation greater than 550 mm (Xu et al., 2010); cold-dry event at 8.2 Cal ka B.P. was also identified. Reconstructed annual precipitations based on the $\delta^{13}C$ of black carbon in Daihai further revealed that the precipitation during the mid-Holocene ranged from less than 170 to 310 mm higher than that at the present. However, the annual precipitation in the early and late Holocene was 70 mm lower than the present (Wang et al., 2013). The content of total organic matter (TOC) also reflected similar results, indicating the high vegetation production and increasing effective precipitations (Sun et al., 2006). All the above records demonstrated the volatility decline after 5 ka. However, our reconstructed results showed that the sediment records missed after 5.2 ka, and the upper layer developed soil humus. We inferred that the upper lacustrine deposit layer may be eroded after the lake declined and the soil humus developed.

Compared with the pollen-based annual precipitation reconstructed from Gonghai Lake located at the fringe of EASM areas controlled by the intensity of EASM (Chen et al., 2015) (Figure 8D), the annual precipitation of Gonghai Lake could represent the most areas of North China and be regarded as an ideal region to evaluate the EASM variability. The reconstructed results demonstrated a gradually intensifying monsoon from 14.7 to 7.0 ka, and a maximum monsoon from 7.8 to 5.3 ka with 30% higher monsoon precipitation than the present. These trends were punctuated by two millennial-scale weakening events which synchronously occurred with the YD event and at 9.5–8.5 ka, which further corresponded to the episodes at ca.10.2, 9, and 8.5–8.1 ka with the declined lake level from Daihai in this study. Since 3.3 ka, a sharp decline occurred in the annual precipitation of Gonghai Lake. Maximum annual precipitation at 7–5 ka during the mid-Holocene revealed the maximum intensity of EASM, which was strongly coupled with the development of Neolithic culture in northern China; for example, Yangshao culture during this period was more prosperous than other Neolithic cultures. Therefore, the strengthening of EASM brought high precipitation with a warm and humid climate, which provided a suitable climate environment for the development of human civilization. Lake-level fluctuations of Daihai corresponded to the EASM variability, which further indicated that the high lake level in Daihai during the Holocene was related to the enhancement of EASM. The evolution pattern of lake-level fluctuations in Daihai was also consistent with the 65°N summer solar insolation variation curve (Berger and Loutre, 1991) (Figure 8A, red line), which could be inferred that the lake-level fluctuation in Daihai was mainly controlled by the intensity of EASM driven by summer solar insolation. The synthesized Northern Hemisphere (30°–90°N) temperature record during the Holocene (Figure 8E) revealed early Holocene (10,000–5,000 years ago) warmth was followed by ~0.7°C cooling through the middle-to-late Holocene (<5,000 years ago), culminating in the coolest temperatures of the Holocene during the Little Ice Age. The high lake level at 5.2 ka was corresponding to the high temperature. However, after 5.2 ka, the lake level declined sharply, while the temperature and annual precipitation variability always displayed a relatively slow descent, which indicated that the lake-level fluctuations nonlinearly responded to the climate

change, and thus, stratigraphic boundaries may not always represent climatic boundaries.

Overall, the lake-level fluctuation of Daihai directly indicates climate change during the early and mid-Holocene. Comparing the lake-level fluctuations with different lakes in the margin of EASM areas and other various regional and global climate signals, we concluded the lake-level fluctuation of Daihai was a regional response to global climate change during the early and mid-Holocene when the climate change is mainly controlled by the EASM driven by solar insolation at high-latitude summer in the Northern Hemisphere. Especially, the high lake level with the high precipitation associated with an intense EASM during the mid-Holocene may have provided a suitable and favorable environment for cultural development, for example, the distribution of the Haishengbulang cultural sites around Daihai at 6.6–5.7 Cal ka B.P. (5.8–5 ka B.P.) with the elevation of 1,290–1,300 m a.s.l. from early to late periods, indicating the expanding lake surface. However, there were 200 years of cultural vacancy during 5.7–5.5 Cal ka B.P. (5.0–4.8 ka B.P.) after the termination of Haishengbulang culture, which might indicate the occurrence of a centennial scale dry event, followed by the emergence of the Laohushan culture. Laohushan culture was a developed primitive agricultural culture with local characteristics around the Daihai Basin, which mainly distributed in the ecotone of agriculture and animal husbandry. Its cultivation was mainly extensive with tools of grindstone knives. However, the sudden collapse of Laohushan culture at 4.8 Cal ka B.P. may be related to the cold events caused by monsoon intensity at the end of the Holocene optimum (Xiao et al., 2019). The decrease in temperature resulted in changes in the heat conditions of agricultural production and the inability to meet the needs of crop growth. People will change their original land-use patterns to adapt to changes in the natural environment, from agriculture-based to semi-agricultural and semi-pastoral or pure animal husbandry. Thus, the ecotone of agriculture and animal husbandry in Daihai basin was developed from then on. Correspondingly, this episode was consistent with the sudden drop of the Daihai lake level after 5.2 ka.

The EASM plays a key role in the evolution of the lake level of Daihai, which is largely consistent with the Gonghai Lake and Dali Lake controlled by the intensity of EASM as well. However, on the centennial scale, the lake-level changes were more complex, which is determined by the regional characteristics of the lake, so the response of different lakes to the EASM intensity could be distinct. For example, the high lake level in the early and mid-Holocene of Dali Lake was not only affected by the EASM driven by solar insolation but also depends on the supply of ice melt and snowmelt.

CONCLUSION

In this study, a series of lakeshore terraces with different heights and braided river deltas around Daihai providing direct geomorphic evidence were used to reconstruct the history of lake-level fluctuations based on the OSL dating method during the early and mid-Holocene. We concluded that the Daihai lake

level was at a relative low level at 10.2 ka. Thereafter, the lake level began to rise at 10.2–8.1 ka, and stayed at a relatively highstand level at 8.1–5.2 ka. Furthermore, the lake level of Daihai reached optimum at 5.2 ka, with ~40 m higher than the modern lake level, and the lake area expanded to about 400 km², approximately six times larger than that of the present. However, the records of the depositional sections revealed that part of the depositional records in the north and east of the Daihai were missed after 5.2 ka, maybe indicating the sudden drop of the lake level of Daihai. The overall climate pattern of Daihai during the early and mid-Holocene shows that the lake level has gradually risen since the early Holocene, and thereafter reached its peak in the mid-Holocene, developing a high lake level, which indicates that the monsoon effective precipitation increased and the humid climate prevailed with the strengthen EASM. The lake-level fluctuations of Daihai during the early and mid-Holocene were mainly controlled by the intensity of EASM. While it is not always synchronous in responding to climate change, which is well confirmed by other lakes at the fringe of ESAM-influenced areas. The local and regional factors are responsible for the fluctuation of the water lake level as well.

DATA AVAILABILITY STATEMENT

The original contributions presented in the study are included in the article/**Supplementary Material**; further inquiries can be directed to the corresponding author.

AUTHOR CONTRIBUTIONS

SH and XC conceived the idea for this article. SH conducted the experiments of Optical Stimulation Luminescence dating and grain

size, led the data statistical analyses, and wrote the manuscript. XC was involved in discussions and contributed to the drafting of the article. All authors approved the final version and agreed to be accountable for the content of the work.

FUNDING

This study was supported financially by the National Natural Science Foundation of China (Nos. 41662011, 41967052, and 61661045) and the Natural Science Foundation of Inner Mongolia (Nos. 2019ZD10 and 2019GG020).

ACKNOWLEDGMENTS

We thank Z. W. Wu and Y. L. Zhang for their help in the field. We are grateful to Prof. H. Long (State Key Laboratory of Lake Science and Environment, Nanjing Institute of Geography and Limnology, Chinese Academy of Sciences) for the discussion of stratigraphic characteristics, and appreciate C. Zhang for improving manuscript. We are particularly grateful to J. Wu (School of Geography and Ocean Science, Nanjing University) for his help with data analysis, graphic drawing, and writing. We also thank the discussion of the sedimentary environment to S. Z. Xin and C. C. Leng. We thank two reviewers for their constructive comments and suggestions which improved the quality of this paper.

SUPPLEMENTARY MATERIAL

The Supplementary Material for this article can be found online at: <https://www.frontiersin.org/articles/10.3389/feart.2021.702843/full#supplementary-material>

REFERENCES

- Aitken, M. J. (1998). *An Introduction to Optical Dating: The Dating of Quaternary Sediments by the Use of Photon-Stimulated Luminescence*. Oxford: Oxford University Press, 1–60.
- Aitken, M. J. (1985). *Thermo Luminescence Dating*. London: Academic Press, 67.
- Arnold, L. J., and Roberts, R. G. (2009). Stochastic Modelling of Multi-Grain Equivalent Dose (De) Distributions: Implications for OSL Dating of Sediment Mixtures. *Quat. Geochronol.* 4, 204–230. doi:10.1016/j.quageo.2008.12.001
- Bailey, R. M., Smith, B. W., and Rhodes, E. J. (1997). Partial Bleaching and the Decay Form Characteristics of Quartz OSL. *Radiat. Measurements* 27, 123–136. doi:10.1016/s1350-4487(96)00157-6
- Berger, A., and Loutre, M. F. (1991). Insolation Values for the Climate of the Last 10 Million Years. *Quat. Sci. Rev.* 10, 297–317. doi:10.1016/0277-3791(91)90033-q
- Botter-Jensen, L., Thomsen, K. J., and Jain, M. (2010). Review of Optically Stimulated Luminescence (OSL) Instrumental Developments for Retrospective Dosimetry. *Radiat. Measurements* 45, 253–257. doi:10.1016/j.radmeas.2009.11.030
- Brennan, B. J., Lyons, R. G., and Phillips, S. W. (1991). Attenuation of Alpha Particle Track Dose for Spherical Grains. *Int. J. Radiat. Appl. Instrumentation. D. Nucl. Tracks Radiat. Measurements* 18, 249–253. doi:10.1016/1359-0189(91)90119-3
- Cao, G., Long, H., Zhang, J., and Lai, Z. (2012). Quartz OSL Dating of Last Glacial Sand Dunes Near Lanzhou on the Western Chinese Loess Plateau: A Comparison between Different Granulometric Fractions. *Quat. Geochronol.* 10, 32–36. doi:10.1016/j.quageo.2011.12.002
- Chen, F., Wu, W., Holmes, J. A., Madsen, D. B., Zhu, Y., Jin, M., et al. (2003). A Mid-holocene Drought Interval as Evidenced by lake Desiccation in the Alashan Plateau, Inner Mongolia, China. *Chin. Sci Bull* 48, 1401–1410. doi:10.1360/03wd0245
- Chen, F., Xu, Q., Chen, J., Birks, H. J. B., Liu, J., Zhang, S., et al. (2015). East Asian Summer Monsoon Precipitation Variability since the Last Deglaciation. *Sci. Rep.* 5, 11186. doi:10.1038/srep11186
- Chen, F., Yu, Z., Yang, M., Ito, E., Wang, S., Madsen, D. B., et al. (2008). Holocene Moisture Evolution in Arid central Asia and its Out-of-phase Relationship with Asian Monsoon History. *Quat. Sci. Rev.* 27, 351–364. doi:10.1016/j.quascirev.2007.10.017
- Chun, X., Qin, F.-Y., Zhou, H.-J., Dan, D., Xia, Y.-Y., and Ulambadrakh, K. (2020). Effects of Climate Variability and Land Use/land Cover Change on the Daihai Wetland of central Inner Mongolia over the Past Decades. *J. Mt. Sci.* 17, 3070–3084. doi:10.1007/s11629-020-6108-1
- Costas, I., Reimann, T., Tsukamoto, S., Ludwig, J., Lindhorst, S., Frechen, M., et al. (2012). Comparison of OSL Ages from Young Dune Sediments with a High-Resolution Independent Age Model. *Quat. Geochronol.* 10, 16–23. doi:10.1016/j.quageo.2012.03.007
- Ding, Z. L., Yu, Z. W., Yang, S. L., Sun, J. M., Xiong, S. F., and Liu, T. S. (2001). Coeval Changes in Grain Size and Sedimentation Rate of Eolian Loess, the Chinese Loess Plateau. *Geophys. Res. Lett.* 28, 2097–2100. doi:10.1029/2000gl006110

- Du, Q., Chang, S., Li, Z., Zhang, L., and Zhang, P. (2013). Holocene lake Sediments and Environmental Changes in Daihai. *Northwest. Geology* 46, 140–147.
- Duller, G. A. T. (2003). Distinguishing Quartz and Feldspar in Single Grain Luminescence Measurements. *Radiat. Measurements* 37, 161–165. doi:10.1016/s1350-4487(02)00170-1
- Fan, A., Li, S.-H., and Chen, Y.-G. (2012). Late Pleistocene Evolution of Lake Manas in Western China with Constraints of OSL Ages of Lacustrine Sediments. *Quat. Geochronol.* 10, 143–149. doi:10.1016/j.quageo.2012.01.007
- Fu, X., Cohen, T. J., and Arnold, L. J. (2017). Extending the Record of Lacustrine Phases beyond the Last Interglacial for Lake Eyre in central Australia Using Luminescence Dating. *Quat. Sci. Rev.* 162, 88–110. doi:10.1016/j.quascirev.2017.03.002
- Goldsmith, Y., Broecker, W. S., Xu, H., Polissar, P. J., Demenocal, P. B., Porat, N., et al. (2017). Northward Extent of East Asian Monsoon Covaries with Intensity on Orbital and Millennial Timescales. *Proc. Natl. Acad. Sci. USA* 114, 1817–1821. doi:10.1073/pnas.1616708114
- Guérin, G., Mercier, N., Nathan, R., Adamiec, G., and Lefrais, Y. (2012). On the Use of the Infinite Matrix assumption and Associated Concepts: A Critical Review. *Radiat. Measurements* 47, 778–785. doi:10.1016/j.radmeas.2012.04.004
- Guo, Y., Huang, C. C., Pang, J., Zhou, Y., Zha, X., and Mao, P. (2017). Reconstruction Palaeoflood Hydrology Using Slackwater Flow Depth Method in the Yanhe River valley, Middle Yellow River basin, China. *J. Hydrol.* 544, 156–171. doi:10.1016/j.jhydrol.2016.11.017
- He, Z., Long, H., Yang, L., and Zhou, J. (2019). Luminescence Dating of a Fluvial Sequence Using Different Grain Size Fractions and Implications on Holocene Flooding Activities in Weihe Basin, central China. *Quat. Geochronol.* 49, 123–130. doi:10.1016/j.quageo.2018.05.007
- Jiang, M., Han, Z., Li, X., Wang, Y., Stevens, T., Cheng, J., et al. (2020). Beach Ridges of Dali Lake in Inner Mongolia Reveal Precipitation Variation during the Holocene. *J. Quat. Sci.* 35, 716–725. doi:10.1002/jqs.3195
- Jin, Z., Li, X., Zhang, B., Han, Y., and Zheng, G. (2013). Geochemical Records in Holocene lake Sediments of Northern China: Implication for Natural and Anthropogenic Inputs. *Quat. Int.* 304, 200–208. doi:10.1016/j.quaint.2013.04.019
- Jin, Z., Wang, S., Shen, J., and Song, J. (2004). Watershed Chemical Weathering and its Response to Climate Events in Daihai Area during Holocene. *Geochimica* 33, 29–36. doi:10.19700/j.0379-1726.2004.01.00410.1080/03009480410001280
- Lai, Z., and Brückner, H. (2008). Effects of Feldspar Contamination on Equivalent Dose and the Shape of Growth Curve for OSL of silt-sized Quartz Extracted from Chinese Loess. *Geochronometria* 30, 49–53. doi:10.2478/v10003-008-0010-0
- Lai, Z., Mischke, S., and Madsen, D. (2014). Paleoenvironmental Implications of New OSL Dates on the Formation of the "Shell Bar" in the Qaidam Basin, Northeastern Qinghai-Tibetan Plateau. *J. Paleolimnol.* 51, 197–210. doi:10.1007/s10933-013-9710-1
- Li, G., Chen, F., Xia, D., Yang, H., Zhang, X., Madsen, D., et al. (2018a). A Tianshan Mountains Loess-Paleosol Sequence Indicates Anti-phase Climatic Variations in Arid central Asia and in East Asia. *Earth Planet. Sci. Lett.* 494, 153–163. doi:10.1016/j.epsl.2018.04.052
- Li, G., Madsen, D. B., Jin, M., Stevens, T., Tao, S., She, L., et al. (2018b). Orbital Scale lake Evolution in the Ejina Basin, central Gobi Desert, China Revealed by K-Feldspar Luminescence Dating of Paleolake Shoreline Features. *Quat. Int.* 482, 109–121. doi:10.1016/j.quaint.2018.03.040
- Li, G., Wang, Z., Zhao, W., Jin, M., Wang, X., Tao, S., et al. (2020a). Quantitative Precipitation Reconstructions from Chagan Nur Revealed Lag Response of East Asian Summer Monsoon Precipitation to Summer Insolation during the Holocene in Arid Northern China. *Quat. Sci. Rev.* 239, 106365. doi:10.1016/j.quascirev.2020.106365
- Li, G., Zhang, H., Liu, X., Yang, H., Wang, X., Zhang, X., et al. (2020b). Paleoclimatic Changes and Modulation of East Asian Summer Monsoon by High-Latitude Forcing over the Last 130,000 Years as Revealed by Independently Dated Loess-Paleosol Sequences on the NE Tibetan Plateau. *Quat. Sci. Rev.* 237, 106283. doi:10.1016/j.quascirev.2020.106283
- Li, H., Liu, Q., and Wang, J. (1992). Study of Evolution of Huangqihai and Daihai lake in Holocene in Inner Mongolia Plateau. *J. Lake Sci.* 4, 31–39.
- Liu, B., Tan, C., Yu, X., Shan, X., and Li, S. (2019). Evolution Model of a Modern delta Fed by a Seasonal River in Daihai Lake, North China: Determined from Ground-Penetrating Radar and Trenches. *Front. Earth Sci.* 13, 262–276. doi:10.1007/s11707-018-0740-x
- Liu, J., Wang, Y., Li, T., Dong, J., Jiang, N., and Tang, W. (2016). Lake Level Fluctuations since 12.5 Cal Ka BP Recorded by Lakeshores of the Dali Lake in Middle-East of Inner Mongolia. *J. Palaeogeogr.* 18, 1044–1052.
- Liu, K., and Lai, Z. P. (2012). Chronology of Holocene Sediments from the Archaeological Salawusu Site in the Mu Us Desert in China and its Palaeoenvironmental Implications. *J. Asian Earth Sci.* 45, 247–255. doi:10.1016/j.jseas.2011.11.002
- Liu, X.-J., Lai, Z., Madsen, D., and Zeng, F. (2015). Last Deglacial and Holocene lake Level Variations of Qinghai Lake, north-eastern Qinghai-Tibetan Plateau. *J. Quat. Sci.* 30, 245–257. doi:10.1002/jqs.2777
- Long, H., Lai, Z., Fuchs, M., Zhang, J., and Li, Y. (2012). Timing of Late Quaternary Palaeolake Evolution in Tengger Desert of Northern China and its Possible Forcing Mechanisms. *Glob. Planet. Change* 92–93, 119–129. doi:10.1016/j.gloplacha.2012.05.014
- Long, H., Lai, Z., Wang, N., and Zhang, J. (2011). A Combined Luminescence and Radiocarbon Dating Study of Holocene Lacustrine Sediments from Arid Northern China. *Quat. Geochronol.* 6, 1–9. doi:10.1016/j.quageo.2010.06.001
- Marcott, S. A., Shakun, J. D., Clark, P. U., and Mix, A. C. (2013). A Reconstruction of Regional and Global Temperature for the Past 11,300 Years. *Science* 339, 1198–1201. doi:10.1126/science.1228026
- Matero, I. S. O., Gregoire, L. J., Ivanovic, R. F., Tindall, J. C., and Haywood, A. M. (2017). The 8.2 Ka Cooling Event Caused by Laurentide Ice Saddle Collapse. *Earth Planet. Sci. Lett.* 473, 205–214. doi:10.1016/j.epsl.2017.06.011
- Murray, A. S., and Olley, J. M. (2002). Precision and Accuracy in the Optically Stimulated Luminescence Dating of Sedimentary Quartz: a Status Review. 21, 1–16.
- Murray, A. S., and Wintle, A. G. (2000). Luminescence Dating of Quartz Using an Improved Single-Aliquot Regenerative-Dose Protocol. *Radiat. Measurements* 32, 57–73. doi:10.1016/S1350-4487(99)00253-X
- Nian, X., Zhang, W., Qiu, F., Qin, J., Wang, Z., Sun, Q., et al. (2019). Luminescence Characteristics of Quartz from Holocene delta Deposits of the Yangtze River and Their Provenance Implications. *Quat. Geochronol.* 49, 131–137. doi:10.1016/j.quageo.2018.04.010
- Peng, Y., Xiao, J., Nakamura, T., Liu, B., and Inouchi, Y. (2005). Holocene East Asian Monsoonal Precipitation Pattern Revealed by Grain-Size Distribution of Core Sediments of Daihai Lake in Inner Mongolia of north-central China. *Earth Planet. Sci. Lett.* 233, 467–479. doi:10.1016/j.epsl.2005.02.022
- Prescott, J. R., and Hutton, J. T. (1994). Cosmic ray Contributions to Dose Rates for Luminescence and ESR Dating: Large Depths and Long-Term Time Variations. *Radiat. Measurements* 23, 497–500. doi:10.1016/1350-4487(94)90086-8
- Roberts, H. M. (2008). The Development and Application of Luminescence Dating to Loess Deposits: a Perspective on the Past, Present and Future. *Boreas* 37, 483–507. doi:10.1111/j.1502-3885.2008.00057.x
- Shen, H., Jia, Y., Zhang, H., Wei, L., and Wang, P. (2006). Environmental Change Inferred from Granular Size Character of Lacustrine Sediment in Inner Mongolia Huangqihai, during 8.022 Ka BP. *Arid Land Geogr.* 29, 457–462.
- Shi, L., Jin, Z., Li, G., Gao, B., and Yan, W. (2014). Depositional Characteristics and Models of the Modern Braided River delta in the Daihai lake, Inner Mongolia. *Nat. Gas Industry* 34, 33–39. doi:10.37811/j.issn.1000-0976.2014.09.005
- Stevens, T., Buylaert, J.-P., Thiel, C., Újvári, G., Yi, S., Murray, A. S., et al. (2018). Ice-volume-forced Erosion of the Chinese Loess Plateau Global Quaternary Stratotype Site. *Nat. Commun.* 9, 983. doi:10.1038/s41467-018-03329-2
- Sun, Q., Wang, S., Zhou, J., Shen, J., Cheng, P., Xie, X., et al. (2009). Lake Surface Fluctuations since the Late Glaciation at Lake Daihai, North central China: A Direct Indicator of Hydrological Process Response to East Asian Monsoon Climate. *Quat. Int.* 194, 45–54. doi:10.1016/j.quaint.2008.01.006
- Sun, Q., and Xiao, J. (2006). Characteristics of the Holocene Optimum in the Monsoon/arid Transition belt Recorded by Core Sediments of Daihai lake, North China. *Quat. Sci.* 26, 781–790.
- Sun, Q., Xiao, J., and Liu, T. (2010). Hydrothermal Status in the Monsoon/arid Transition belt of China since the Last Glaciation Inferred from Geochemical Characteristics of the Sediment Cores at Daihai lake. *Quat. Sci.* 30, 1121–1130.
- Sun, Q., Zhou, J., Shen, J., Chen, P., Wu, F., and Xie, X. (2006). Environmental Characteristics of Mid-holocene Recorded by Lacustrine Sediments from Lake Daihai, north Environment Sensitive Zone, China. *Sci. China Ser. D* 49, 968–981. doi:10.1007/s11430-006-0968-2
- Thomsen, K. J., Jain, M., Murray, A. S., Denby, P. M., Roy, N., and Bøtter-Jensen, L. (2008). Minimizing Feldspar OSL Contamination in Quartz UV-OSL Using

- Pulsed Blue Stimulation. *Radiat. Measurements* 43, 752–757. doi:10.1016/j.radmeas.2008.01.020
- Wang, S., Wu, R., and Jaing, X. (1990). Environment Evolution and Paleoclimate of Daihai lake, Inner Mongolia since the Last Glaciation. *Quat. Sci.*, 223–232.
- Wang, X., Cui, L., Xiao, J., and Ding, Z. (2013). Stable Carbon Isotope of Black Carbon in lake Sediments as an Indicator of Terrestrial Environmental Changes: An Evaluation on Paleorecord from Daihai Lake, Inner Mongolia, China. *Chem. Geology* 347, 123–134. doi:10.1016/j.chemgeo.2013.03.009
- Wintle, A. G., and Murray, A. S. (2006). A Review of Quartz Optically Stimulated Luminescence Characteristics and Their Relevance in Single-Aliquot Regeneration Dating Protocols. *Radiat. Measurements* 41, 369–391. doi:10.1016/j.radmeas.2005.11.001
- Wu, J., Lu, H., Yi, S., Xu, Z., Gu, Y., Liang, C., et al. (2019). Establishing a High-Resolution Luminescence Chronology for the Zhenbeitai Sand-Loess Section at Yulin, North-Central China. *Quat. Geochronol.* 49, 78–84. doi:10.1016/j.quageo.2018.03.013
- Xiao, J., Chang, Z., Si, B., Qin, X., Itoh, S., and Lomtatidze, Z. (2009). Partitioning of the Grain-Size Components of Dali Lake Core Sediments: Evidence for lake-level Changes during the Holocene. *J. Paleolimnol.* 42, 249–260. doi:10.1007/s10933-008-9274-7
- Xiao, J., Fan, J., Zhai, D., Wen, R., and Qin, X. (2015). Testing the Model for Linking Grain-Size Component to lake Level Status of Modern Clastic Lakes. *Quat. Int.* 355, 34–43. doi:10.1016/j.quaint.2014.04.023
- Xiao, J., Fan, J., Zhou, L., Zhai, D., Wen, R., and Qin, X. (2013). A Model for Linking Grain-Size Component to lake Level Status of a Modern Clastic lake. *J. Asian Earth Sci.* 69, 149–158. doi:10.1016/j.jseas.2012.07.003
- Xiao, J., Si, B., Zhai, D., Itoh, S., and Lomtatidze, Z. (2008). Hydrology of Dali Lake in central-eastern Inner Mongolia and Holocene East Asian Monsoon Variability. *J. Paleolimnol.* 40, 519–528. doi:10.1007/s10933-007-9179-x
- Xiao, J., Xu, Q., Nakamura, T., Yang, X., Liang, W., and Inouchi, Y. (2004). Holocene Vegetation Variation in the Daihai Lake Region of north-central China: a Direct Indication of the Asian Monsoon Climatic History. *Quat. Sci. Rev.* 23, 1669–1679. doi:10.1016/j.quascirev.2004.01.005
- Xiao, J., Zhang, S., Fan, J., Wen, R., Xu, Q., Inouchi, Y., et al. (2019). The 4.2 Ka Event and its Resulting Cultural Interruption in the Daihai Lake basin at the East Asian Summer Monsoon Margin. *Quat. Int.* 527, 87–93. doi:10.1016/j.quaint.2018.06.025
- Xu, J., Jia, Y., Lai, Z., Wang, P., Xu, M., and Shen, H. (2012). Climate Variations during Early to Mid-holocene in Huangqihai Lake in Northern China Based on the Lake Deposit Analysis. *Acta Sedimentologica Sinica* 30, 731–738. doi:10.14027/j.cnki.cjxb.2012.04.021
- Xu, Q., Xiao, J., Li, Y., Tian, F., and Nakagawa, T. (2010). Pollen-Based Quantitative Reconstruction of Holocene Climate Changes in the Daihai Lake Area, Inner Mongolia, China. *J. Clim.* 23, 2856–2868. doi:10.1175/2009jcli3155.1
- Xu, Q., Xiao, J., Nakamura, T., Yang, X., Zheng, Z., Liang, W., et al. (2004). Pollen Evidence of Vegetation and Climate Changes in Daihai lake Area during the Holocene. *J. Glaciology Geocryology* 26, 73–80.
- Yu, L., and Lai, Z. (2017). Holocene Climate Change Inferred from Stratigraphy and OSL Chronology of Aeolian Sediments in the Qaidam Basin, Northeastern Qinghai-Tibetan Plateau. *Quat. Res.* 81, 488–499. doi:10.1016/j.yqres.2013.09.006
- Yu, X., Li, S., Tan, C., Xie, J., Chen, B., and Yang, F. (2013). The Response of Deltaic Systems to Climatic and Hydrological Changes in Daihai Lake Rift basin, Inner Mongolia, Northern China. *J. Palaeogeogr.* 2, 41–45. doi:10.3724/SP.J.1261.2013.00016
- Zhang, J., Jia, Y., Lai, Z., Long, H., and Yang, L. (2011). Holocene Evolution of Huangqihai Lake in Semi-arid Northern China Based on Sedimentology and Luminescence Dating. *The Holocene* 21, 1261–1268. doi:10.1177/0959683611405232
- Zhang, J., Lai, Z., and Jia, Y. (2012). Luminescence Chronology for Late Quaternary lake Levels of Enclosed Huangqihai lake in East Asian Monsoon Marginal Area in Northern China. *Quat. Geochronol.* 10, 123–128. doi:10.1016/j.quageo.2012.04.015
- Zhang, J., Tsukamoto, S., Jia, Y., and Frechen, M. (2016). Lake Level Reconstruction of Huangqihai Lake in Northern China since MIS 3 Based on Pulsed Optically Stimulated Luminescence Dating. *J. Quat. Sci.* 31, 225–238. doi:10.1002/jqs.2861
- Zhang, Z., and Wang, S. (2000). Paleoclimate Significance of Lake Level Fluctuation, Oeat Development and Eolian Sand-Paleosoil Series in Hulun Lake. *J. Arid Land Resour. Environ.* 14, 56–59.
- Zhao, X., Huang, C. C., Pang, J., Zha, X., Guo, Y., and Hu, G. (2016). Holocene Climatic Events Recorded in Palaeoflood Slackwater Deposits along the Middle Yiluohe River valley, Middle Yellow River basin, China. *J. Asian Earth Sci.* 123, 85–94. doi:10.1016/j.jseas.2016.04.002

Conflict of Interest: The authors declare that the research was conducted in the absence of any commercial or financial relationships that could be construed as a potential conflict of interest.

Publisher's Note: All claims expressed in this article are solely those of the authors and do not necessarily represent those of their affiliated organizations, or those of the publisher, the editors and the reviewers. Any product that may be evaluated in this article, or claim that may be made by its manufacturer, is not guaranteed or endorsed by the publisher.

Copyright © 2021 Huang and Chun. This is an open-access article distributed under the terms of the Creative Commons Attribution License (CC BY). The use, distribution or reproduction in other forums is permitted, provided the original author(s) and the copyright owner(s) are credited and that the original publication in this journal is cited, in accordance with accepted academic practice. No use, distribution or reproduction is permitted which does not comply with these terms.